Synchronous Reluctance Motor/Alternator for Flywheel Energy Storage Systems

Heath Hofmann Seth R. Sanders
Department of Electrical Engineering and Computer Science
University of California, Berkeley

Abstract— This paper presents a synchronous reluctance machine design for high-speed high-power applications, such as the motor/alternator for a flywheel energy storage system. The rotor consists of alternating layers of ferromagnetic and nonmagnetic steel that are joined together by a process known as explosion bonding. Analytical expressions for the direct and quadrature inductances of the machine are presented, and are then used to optimize machine design. These expressions compare well with results obtained from finite element analysis. Structural and electrical analyses of a 60kW, 48,000 r.p.m. machine indicate that the design will be appropriate for flywheel systems. Current work involves construction and testing of the above design.

I. Introduction

The development of flywheel energy storage devices for use in electric/hybrid electric vehicles has become an important area of research. The high efficiency and power density of flywheel devices will allow them to serve as load-levelling devices for the electrochemical batteries of a vehicle, or perhaps to replace the batteries themselves. It is typically envisioned that energy will be transferred into and out of the flywheel electrically via a motor/alternator. Primary design considerations for the motor/alternator are:

- High output power capability,
- Ability of the rotor to withstand high speeds,
- Negligible zero-torque spinning losses,
- High reliability,
- High efficiency, and
- Low cost.

In this paper we present a synchronous reluctance machine design aimed at flywheel energy storage systems and other high-speed, high-power applications. We first discuss the advantages of synchronous reluctance machines with respect to permanent magnet machines for this particular application. We then present a synchronous reluctance machine design and describe its construction. Next we analyze the structural and electrical characteristics of a prototype design rated at 60kW and 48,000 r.p.m. Finally we estimate the performance of this design in high-speed, high-power applications. Ongoing work includes construction and testing of the above prototype design.

II. Machine Selection

A. Permanent Magnet Machines

Most (if not all) flywheel systems discussed in the literature use a permanent magnet machine as the motor/alternator [1-3]. Permanent magnet machines are a popular choice due to the high efficiency that can be obtained since no power loss is associated with machine excitation. Permanent magnet machines also typically have a high power/weight ratio when compared with other machines. In order to achieve high power levels these designs typically use magnets with high energy products, such as neodymium-iron-boron. There are, however, several disadvantages in using permanent magnet machines for this particular application:

- If the magnitude of the magnetic field inside a permanent magnet exceeds the intrinsic coercivity of the material (e.g., due to excessive armature reaction), the material demagnetizes. When this occurs the machine is inoperable until the magnets can be remagnetized, which typically involves disassembly of the machine. Furthermore, the intrinsic coercivity of permanent magnets is markedly affected by temperature, thereby increasing the possibility of demagnetization. For example, the intrinsic coercivity of neodymium-iron-boron decreases by a factor greater than 2 as the temperature of the magnet increases from $20°C$ to $100°C$ [4].
- Permanent magnet materials with high energy products can be prohibitively expensive in high-power applications. In a study of the feasibility of using flywheels to power electric vehicles [2], researchers at Lawrence Livermore National Laboratory estimated the cost of neodymium-iron-boron magnets to be $85 per pound, and they further state that they find no basis to assume these costs will be reduced in the near future. Attempts at design optimization to minimize magnet volume must take into account a safety factor in order to prevent demagnetization [5].
- Permanent magnet machines with iron in the stator experience significant zero-torque electromagnetic spinning losses due to the constant permanent

0-7803-3292-X/96/$5.00

magnet field excitation. This problem can be resolved with the design of "ironless" machines (machines without any iron in the stator). However, for a given magnet volume "ironless" machines have substantially lower air-gap flux densities, and hence lower power levels, than do machines with iron in the stator.

- Permanent magnet machines require rotor structures which support the magnets against the large centrifugal forces experienced during high-speed operation. This significantly constrains the design of high-speed, high-power rotors.

The combination of these properties of permanent magnet machines makes design of a low-cost, high-reliability motor/alternator for flywheel applications particularly challenging.

B. Synchronous Reluctance Machines

Synchronous reluctance machines have the following advantages over permanent magnet machines:

- There is no concern with demagnetization, hence synchronous reluctance machines are inherently more reliable than permanent magnet machines.
- There need be no excitation field at zero torque, thus eliminating electromagnetic spinning losses.
- Synchronous reluctance machine rotors can be constructed entirely from high-strength, low-cost materials.

The ideal synchronous reluctance machine is typified by having a rotor whose structure is such that the inductance of the stator windings in the $dq0$ reference frame [13] varies sinusoidally from a maximum value L_d (direct inductance) to a minimum value L_q (quadrature inductance) as a function of angular displacement of the rotor. A figure of merit for the synchronous reluctance machine is the ratio of direct inductance to quadrature inductance, L_d/L_q. For example, the maximum achievable power factor PF_{max} of a synchronous reluctance machine is given by

$$PF_{max} = \frac{L_d/L_q - 1}{L_d/L_q + 1}. \qquad (1)$$

Higher L_d/L_q ratios yield higher power factors, which corresponds to reduced I^2R losses and reduced volt-ampere ratings of the inverter driving the machine.

There are many approaches to constructing synchronous reluctance rotors. One is to give the rotor a salient shape such that the quadrature air gap is much larger than the direct air gap, as shown in Fig. 1(a). This approach yields relatively small L_d/L_q ratios in the range of 2-3. These low ratios are largely the result of circulating

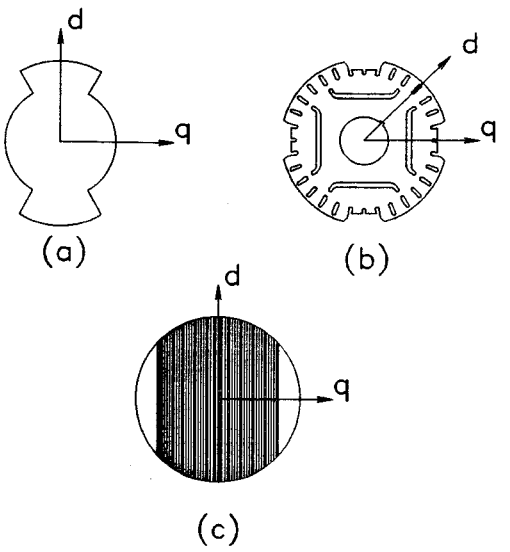

Fig. 1. Synchronous reluctance rotor designs: (a) Salient rotor (b) Laminated rotor (c) Axially-laminated rotor

flux in the pole faces of the rotor [6]. However, the ruggedness and simplicity of the rotor structure has encouraged study of this approach for high-speed applications [7].

Another approach is to use laminations with "flux barriers" punched into the steel, as shown in Fig. 1(b) for a 4-pole machine. However, these flux barriers (and the central hole of the lamination required for the shaft) weaken the rotor structurally, and thus make this approach a poor choice for high-speed design.

Yet another approach is to laminate the rotor in the axial direction, as shown in Fig. 1(c). A two-pole, 2hp axially-laminated machine with an L_d/L_q ratio of 20 and a maximum efficiency of 94% (@3,600 r.p.m.) has been reported in the literature [8]. However, it is difficult to design a rotor capable of containing these laminations at high speeds.

Our approach to rotor design is shown in Fig. 2. In this case, the rotor consists of alternating layers of ferromagnetic and nonmagnetic steel. We choose the thicknesses of the steels such that the pitch of the ferromagnetic rotor segments matches the slot pitch of the stator. In this way, the ferromagnetic rotor segments always "see" a stator tooth pitch regardless of the angle of rotation of the rotor. This is done to minimize flux variations, and hence iron losses, in the rotor, and is discussed in more detail in [9].

III. Rotor Construction

To construct the rotor we are using a joining technique known as explosion bonding. Explosion bonding uses explosive energy to force two or more metal sheets together at high pressures, as shown in Fig. 3. Conventional, inexpensive explosives are adequate for this process. The high pressures cause several atomic layers on the surface

0-7803-3292-X/96/$5.00

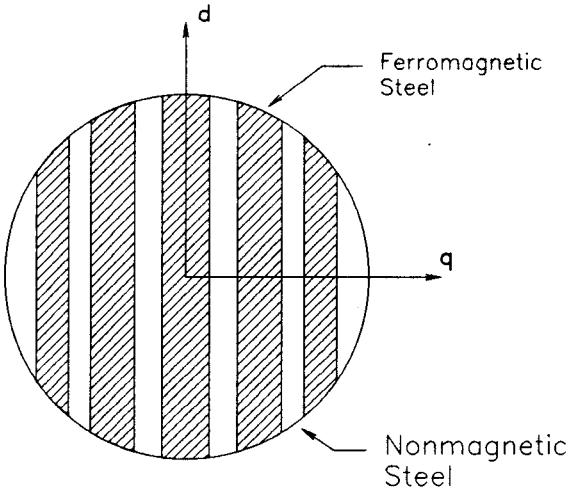

Fig. 2. New Synchronous Reluctance Rotor Design

of each sheet to behave as a fluid. The angle of collision between the two metals forces this fluid to jet outward - effectively scrub-cleaning the metal surfaces. These ultra-clean surfaces, along with the high pressures forcing the metal plates together, provide the necessary conditions for solid-phase welding [10].

Experimental tests [11] on a stainless steel/mild steel bond indicate that the tensile and fatigue strengths of the bond are greater than those of either of the component materials, due to the shock hardening which occurs during the process. The bond was also subjected to 10 cycles of temperature variation from $20°C - 700°C$, with no significant reduction in tensile strength.

We note that other joining techniques, such as brazing, roll bonding, or diffusion bonding may also be appropriate for rotor construction.

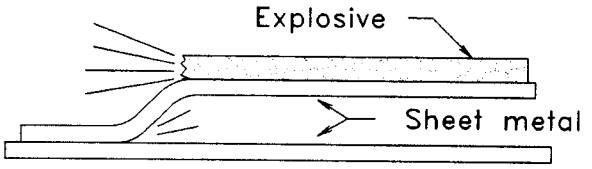

Fig. 3. Explosion Bonding

The envisioned rotor construction process is shown in Fig. 4. First, sheets of ferromagnetic and nonmagnetic steel are bonded together as described above. The bonded sheets are then cut into rectangular blocks, which are machined into the desired rotors. The rotor shaft can also be machined out of the same block as the rotor.

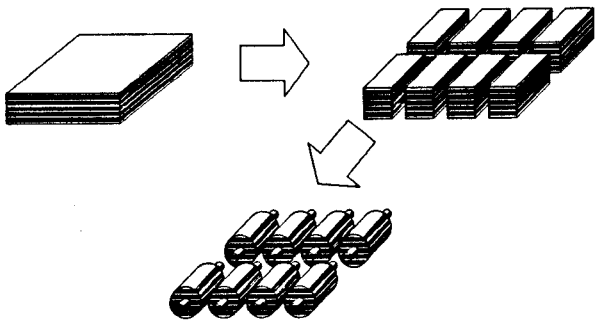

Fig. 4. Envisioned Rotor Construction Process

IV. Prototype Design

In our prototype design the nonmagnetic steel (Nitronic 50) is a specialty steel with a yield strength of 75 ksi and a tensile strength of 120 ksi, and can be purchased in small quantities for \$6/lb. The ferromagnetic steel is an inexpensive carbon steel (4140), which can achieve yield strengths as high as 250 ksi when heat treated. These materials were chosen for their magnetic properties, high yield strengths, and high ductility (which is required for the explosion bonding process).

The number of poles of the machine is constrained to be two due to the construction process. However, there are other advantages in using a two-pole machine in flywheel applications. Higher-pole machine rotors can experience substantial electromagnetic radial forces generated by the stator winding. These are due to the net attractive force experienced by the poles of a pole-pair to the stator. In a two-pole configuration, however, the two poles are directly opposite one another, and hence the net force on the rotor is approximately zero. Elimination of these forces may substantially reduce load requirements on the bearings of the system, which is particularly important if magnetic bearings are used. Furthermore, higher L_d/L_q ratios can be obtained with two-pole rotors as opposed to higher-pole rotors [5].

Table I presents parameters for a prototype design that is currently under construction. Variables are provided for certain parameters, and will be used in the following analyses.

A. Structural Analysis

In the following we assume the rotor to be a solid cylinder with uniform structural properties, due to the assumed completeness of the bond between the nonmagnetic and ferromagnetic steels and the approximate equivalence of the density, modulus of elasticity, and Poisson's ratio of

Parameter	Value
Stator Outer Diameter:	6.0 in.
Stack Length (ℓ_s):	4.375 in.
Stator Laminations:	M-15 Non-Oriented Silicon Steel (14 mil thickness)
# Turns/Phase (N):	24
Rotor Diameter (d):	3.3 in.
Air Gap (g):	0.025 in.
# Poles:	2
Projected Speed Range (ω):	24,000-48,000 r.p.m.
Total Weight of Machine:	35 lbs.

TABLE I
SYNCHRONOUS RELUCTANCE MOTOR/ALTERNATOR DESIGN

the two materials. The maximum stress in a cylinder of diameter d, density ρ, and Poisson's ratio ν that is rotating at an angular velocity ω is presented in [12]:

$$\sigma_{max} = \rho\omega^2 d^2 \frac{3-2\nu}{32\,(1-\nu)}. \tag{2}$$

Using this formula, the maximum stress in a 3.3 in. diameter rotor spinning at a rotational speed of 48,000 r.p.m. will be 21 ksi, which is substantially lower than the yield strengths of either steel.

B. Electrical Analysis

The direct and quadrature inductances in the $dq0$ reference frame can be written as [13]:

$$\begin{aligned} L_d &= \frac{3}{2}L_{dm} + L_\ell \\ L_q &= \frac{3}{2}\left(L_{qmf} + L_{qmc}\right) + L_\ell, \end{aligned} \tag{3}$$

where L_{dm} is the single-phase direct magnetizing inductance and L_ℓ is the single-phase leakage inductance. The single-phase quadrature magnetizing inductance has two components: L_{qmf}, the flow-through magnetizing inductance, and L_{qmc}, the circulating magnetizing inductance. These two inductances are described more fully in the following.

To estimate the flow-through magnetizing inductances (L_{dm} and L_{qmf}), we create a magnetic circuit consisting of reluctances between all ferromagnetic materials in the machine, as shown in Fig. 5. Ferromagnetic materials are considered to be infinitely permeable to simplify analysis. We assume a smooth air gap between the rotor and the stator, and sinusoidal excitation.

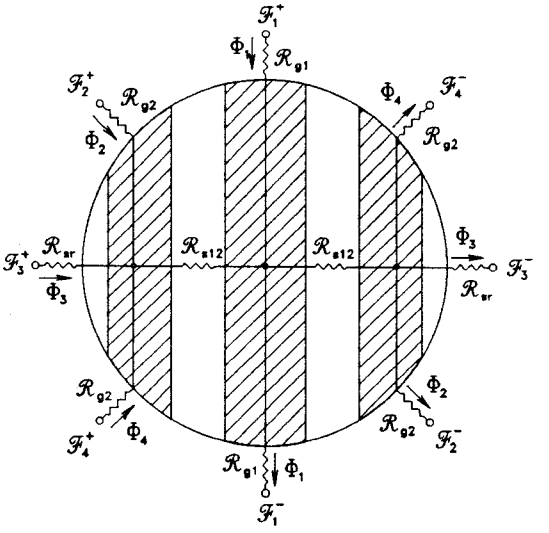

Fig. 5. Magnetic Circuit of Synchronous Reluctance Machine

The reluctances terminating at the stator can be considered to be connected to magnetomotive forces $\mathcal{F}_i^{\pm}$, which in the case of single-phase excitation have the relation

$$\mathcal{F}_i = \mathcal{F}_i^+ - \mathcal{F}_i^- = NI\cos(\varphi_i + \varphi_r), \tag{4}$$

where I is the phase current, φ_r is the angle between the direct axis of the rotor and the axis of maximum magnetic potential from the excited winding, and φ_i is the angle between the direct axis of the rotor and the pole face of the ith ferromagnetic segment, as shown in Fig. 6. Direct and quadrature excitation of the rotor correspond to $\varphi_r = 0°$ and $\varphi_r = 90°$, respectively.

The magnetomotive forces $\mathcal{F}_i$ and the gap fluxes Φ_i are then related by

$$\underline{\mathcal{F}} = \underline{\mathcal{R}}\,\underline{\Phi}, \tag{5}$$

where

$$\underline{\mathcal{F}} = \begin{bmatrix} \mathcal{F}_1 \\ \vdots \\ \mathcal{F}_n \end{bmatrix}, \quad \underline{\Phi} = \begin{bmatrix} \Phi_1 \\ \vdots \\ \Phi_n \end{bmatrix}, \tag{6}$$

and $\underline{\mathcal{R}}$ is a reluctance matrix, whose elements $\mathcal{R}_{ij}$ are determined as follows:

$$\mathcal{R}_{ij} = \frac{\mathcal{F}_i}{\phi_j}\Big|_{\Phi_k=0, k\neq j}. \tag{7}$$

For example, for a rotor with 3 ferromagnetic segments as shown in Fig. 5, the reluctance matrix is:

$$\underline{\mathcal{R}} = 2\begin{bmatrix} \mathcal{R}_{g1} & 0 & 0 & 0 \\ 0 & \mathcal{R}_{g2}+\mathcal{R}_{s12} & \mathcal{R}_{s12} & \mathcal{R}_{s12} \\ 0 & \mathcal{R}_{s12} & \mathcal{R}_{sr}+\mathcal{R}_{s12} & \mathcal{R}_{s12} \\ 0 & \mathcal{R}_{s12} & \mathcal{R}_{s12} & \mathcal{R}_{g2}+\mathcal{R}_{s12} \end{bmatrix} \tag{8}$$

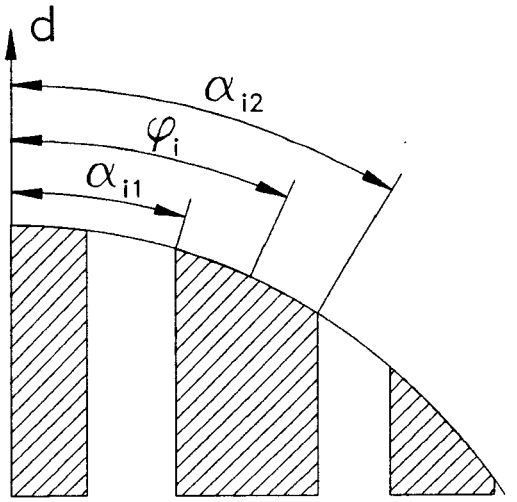

Fig. 6. Angular Parameters of ith Segment

Using this vector notation, the magnetic energy stored in the rotor can be shown to be

$$W_m = \frac{1}{2}\underline{\Phi}^T \underline{\mathcal{R}}\,\underline{\Phi} \quad (9)$$

$$= \frac{1}{2}\underline{\mathcal{F}}^T \underline{\mathcal{R}}^{-1}\underline{\mathcal{F}}, \quad (10)$$

and therefore the flow-through magnetizing inductance for a given orientation of the rotor can be determined:

$$L_{\theta m} = \frac{2W_m}{I^2} = \frac{\underline{\mathcal{F}}^T \underline{\mathcal{R}}^{-1}\underline{\mathcal{F}}}{I^2} \quad (11)$$

Hence L_{dm} and L_{qmf} can be calculated using (11) by setting $\varphi_r = 0°$ and $\varphi_r = 90°$, respectively.

The circulating quadrature inductance, L_{qmc}, corresponds to the component of quadrature flux which circulates in the pole faces of the ferromagnetic segments, and is described more fully in [6]. The derivation of L_{qmc} for our rotor design is long but straightforward, and hence we provide only the result:

$$L_{qmc} = \sum_i L_{qmc\,i}, \quad (12)$$

where $L_{qmc\,i}$ corresponds to the ith ferromagnetic segments from the center. If the segment is in the center of the rotor, we have

$$L_{qmc\,1} = \frac{\mu_0 d \ell_s N^2}{4g}\left(\sin(2\alpha_{12}) - 2\alpha_{12} + 4\frac{(1-\cos(\alpha_{12}))^2}{\alpha_{12}}\right) \quad (13)$$

where α_{12} represents the angular location of the edge of the center segment with respect to the direct axis. Otherwise,

$$L_{qmc\,i} = \frac{\mu_0 d \ell_s N^2}{8g}(\sin(2\alpha_{i2}) - \sin(2\alpha_{i1}) - 2(\alpha_{i2} - \alpha_{i1}) + 4\left(\cos(\alpha_{i2}) - \cos(\alpha_{i1})\right)^2/(\alpha_{i2} - \alpha_{i1})) \quad (14)$$

where α_{i1} and α_{i2} are the angular coordinates of the edges of the ith ferromagnetic segment from the center, as shown in Fig. 6.

The leakage inductance L_ℓ of the machine can be divided into two parts:

$$L_\ell = L_{\ell slot} + L_{\ell end}, \quad (15)$$

where $L_{\ell slot}$ is the inductance due to the conductors in the slots of the stator and $L_{\ell end}$ is the inductance due to the end turns of the stator winding. Our calculation of the slot leakage inductance is based on a two-dimensional finite element analysis of a stator with no rotor. The fraction of leakage inductance due to the end turns is estimated by taking leakage inductance measurements on the stator of a two-pole, 3 hp induction machine with similar dimensions to the above design, and subtracting the slot leakage inductance (which we determine by finite element analysis). The results of this analysis suggest that $L_{\ell end}$ comprises approximately 25% of L_ℓ.

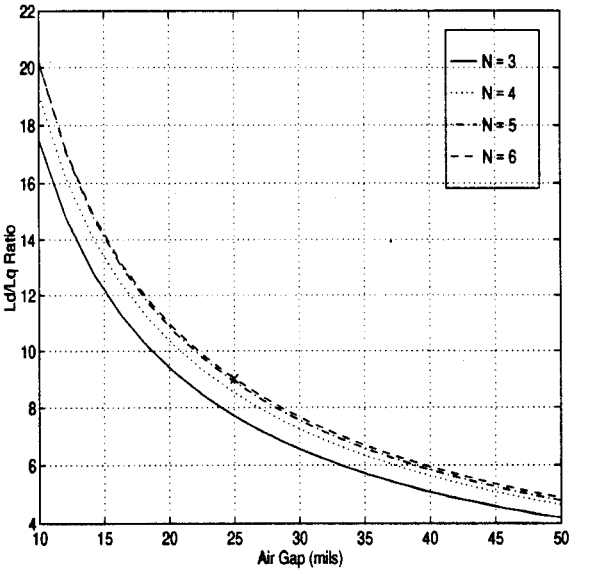

Fig. 7. Optimized L_d/L_q ratio as a function of air gap and number of ferromagnetic rotor segments. The 'x' corresponds to ratio calculated using two-dimensional finite element analysis on a prototype design.

Using the analytical model we optimize the L_d/L_q ratio with respect to the locations of the ferromagnetic segments in the rotor. We constrain the thicknesses of the ferromagnetic segments such that the pitch of their pole

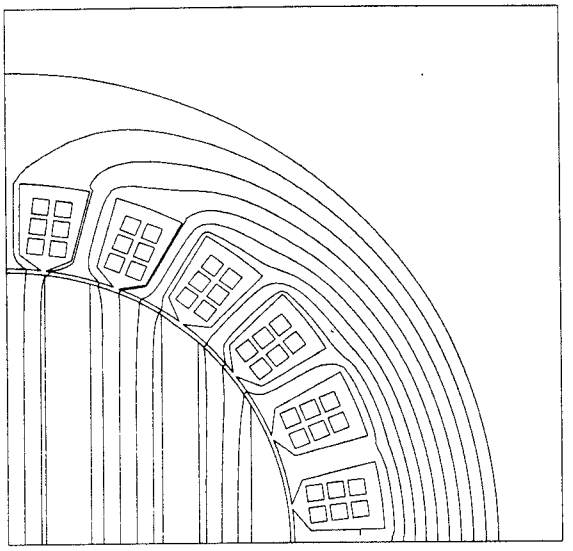

Fig. 8. 2-D Finite Element Analyis of Direct Flux, Prototype Design.

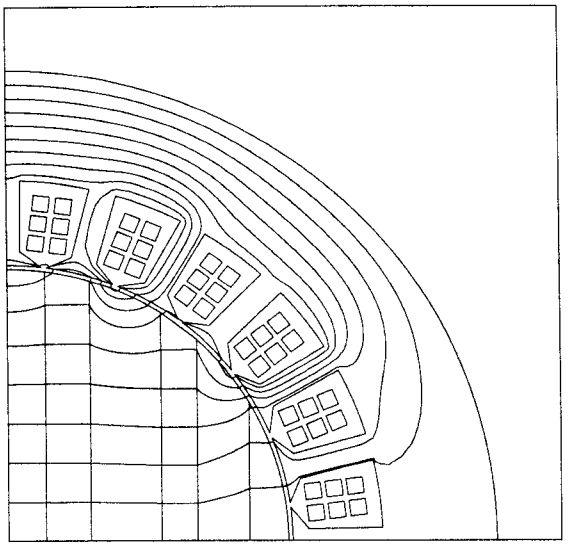

Fig. 9. 2-D Finite Element Analyis of Quadrature Flux, Prototype Design.

	Analytical	Finite Element
Direct Inductance:	$3.91mH$	$4.14mH$
Quadrature Inductance:	$440\mu H$	$459\mu H$
L_d/L_q Ratio:	8.9	9.0

TABLE II
COMPARISON BETWEEN ANALYTICAL FORMULAS AND FINITE-ELEMENT ANALYSIS, FIVE SEGMENT ROTOR, 25-MIL GAP

faces are a fixed value, in this case equal to the slot pitch of the stator. Plots of optimized L_d/L_q ratios as a function of gap length and number of ferromagnetic segments are shown in Fig. 7.

To validate the above model we performed two-dimensional finite element analysis on a five-segment, 25-mil gap design. Plots of the flux contours for both direct and quadrature excitation are shown in Figs. 8 and 9, respectively. Results of both the analytical and finite element methods are shown in Table II, where the finite element results were adjusted to account for end-turn leakage inductance.

V. ESTIMATED PERFORMANCE OF PROTOTYPE DESIGN

The power output of a two-pole synchronous reluctance machine is given by [5]:

$$P_{out} = \frac{3}{2}V^2\frac{\omega(L_d-L_q)}{(\omega^2 L_d L_q + R_s^2)^2}[(\omega^2 L_d L_q - R_s^2)\sin(2\delta) + R_s\omega(L_d+L_q)\cos(2\delta) - R_s\omega(L_d-L_q)], \quad (16)$$

where V is the rms phase voltage and δ is an angle which at high speeds closely approximates the angle between the direct axis of the rotor and the location of maximum flux density in the air gap. In normal operation δ varies between 0° and 45°.

The stator resistance R_s is calculated using the formula:

$$R_s = \frac{K_e}{K_p}\frac{12\rho_{Cu}\ell_s N^2}{A_c}, \quad (17)$$

where ρ_{Cu} is the resistivity of copper, A_c is the total available copper area in the stator, and K_e and K_p are coefficients which take into account the end turns and packing factor of the conductors, respectively.

Our value of $\frac{K_e}{K_p}$ is based on measurements performed on a two-pole, 3 hp induction machine with similar dimen-

sions to the prototype design. We assume an operating temperature of $120°C$ when determining ρ_{Cu}.

A. Copper Losses

An analytical expression for copper (I^2R) losses can be derived from formulas presented in [5]:

$$\begin{aligned} P_{Cu} &= 3I^2R_s \\ &= \frac{3V^2R_s}{\left(R_s^2+\omega^2L_dL_q\right)^2}[R_s^2+R_s\omega(L_d-L_q)\sin(2\delta) \\ &\quad +\omega^2\left((L_d^2+L_q^2)/2-(L_d^2-L_q^2)/2\cos(2\delta)\right)] \end{aligned} \tag{18}$$

There will also be copper losses in the conductors due to proximity effect and skin effect. We do not include these losses in our analysis, noting that there are methods of alleviating these losses (the use of Litz wire, for example).

B. Core Losses

To estimate stator iron losses, we take core loss data for 14-mil, M-15 silicon steel at 400 Hz and perform a least squares fit to a B^2 curve, where B represents maximum flux density in the steel. For core losses at different frequencies we conservatively assume that the losses increase proportionately with f^2. We calculate maximum flux densities throughout the stator, and integrate to find total core loss:

$$P_{core}(f) = \left(\frac{f}{400}\right)^2 \int_V K_{fit}B(V)^2dV \tag{19}$$

We calculate core losses corresponding only to the fundamental component of flux density in the stator iron, noting that there will also be significant core losses in the stator and rotor due to the winding and slot harmonics. These losses are difficult to estimate reliably, and are therefore not included in this analysis.

Figs. 10 and 11 present the above core and copper losses as a function of output power at rotational speeds of 48,000 r.p.m. and 24,000 r.p.m., respectively. The operating point of the machine was chosen to minimize the sum of these losses for a given output power. The increase in losses at high power levels corresponds to adjustment of the operating point in order to avoid saturation of the stator teeth.

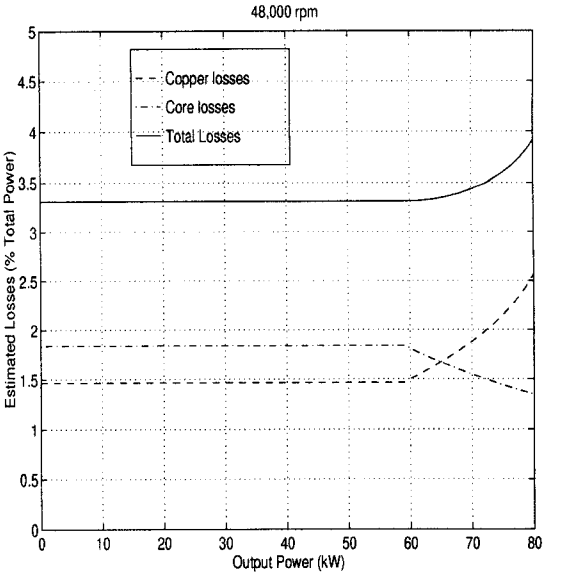

Fig. 10. Estimated Losses in Synchronous Reluctance Machine Operating at 48,000 r.p.m.

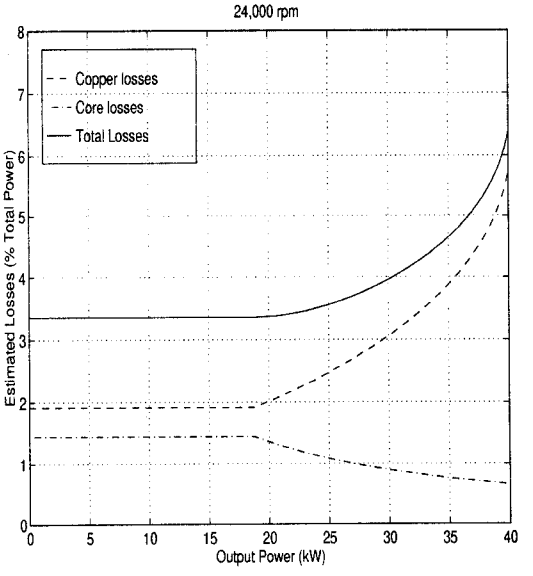

Fig. 11. Estimated Losses in Synchronous Reluctance Machine Operating at 24,000 r.p.m.

VI. Experimental Setup

We are currently in the process of constructing an experimental setup to test the above machine design. A schematic of the setup is shown in Fig. 12. Two identical machines will be connected at the shaft. High-efficiency 60 kW MOSFET inverters, both connected to a common voltage bus, have been constructed to drive the machines. Driving one machine as a motor and the other as a generator causes power to flow in a loop, as shown in Fig. 12. An external power source will be used to supply the necessary power to keep the machines at a given steady-state operating point. This power will be equivalent to the total losses in the system, and will therefore allow us to determine the efficiency of the machines with a high degree of accuracy.

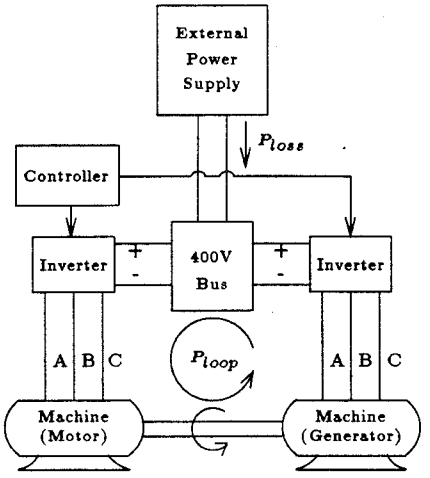

Fig. 12. Experimental setup

VII. Conclusion

We have presented a high-power, high-speed synchronous reluctance machine design. Estimated performance suggests that this machine will be appropriate for use as a motor/alternator in a flywheel energy storage system for electric/hybrid electric vehicles. We expect this design to have the advantages of greater reliability and lower unit cost than permanent magnet machines.

References

[1] Abacus Technology Corporation. Technology assessments of advanced energy storage systems for electric and hybrid vehicles. Technical Report DE93-014395, U.S. Department of Energy Office of Transportation Technologies, April 1993. NTIS Document.

[2] Lawrence Livermore National Laboratory. Feasibility of electromechanical batteries for electric vehicles. Technical Report DE92-015172, U.S. Department of Commerce, May 1992. NTIS Document.

[3] P.P. Acarnley, B.C. Mecrow, J.S. Burdess, J.N. Fawcett, J.G. Kelly, and P.G. Dickinson. Design principles for a flywheel energy store for road vehicles. In *Conference Record of the 30th IAS Annual Meeting*, pages 672–678, 1995.

[4] P. Campbell. *Permanent Magnet Materials and Their Application.* Cambridge University Press, 1994.

[5] S.A. Nasar, I. Boldea, and L.E. Unnewehr. *Permanent Magnet, Reluctance, and Self-Synchronous Motors.* CRC Press, 1993.

[6] T.A. Lipo, A. Vagati, L. Malesani, and T. Fukao. Synchronous reluctance motors and drives - a new alternative. Tutorial Presented at the 26th IEEE IAS Annual Meeting, October 1992.

[7] T. Fukao, A. Chiba, and M. Matsui. Test results on a super-high-speed amorphous-iron reluctance motor. *IEEE Transactions on Industry Applications*, 25(1):119–125, January/February 1989.

[8] I. Boldea, Z. Fu, and S.A. Nasar. Performance evaluation of axially-laminated anisotropic (ala) rotor reluctance synchronous motors. *IEEE Transactions on Industry Applications*, 30(4):977–85, July-Aug. 1994.

[9] A. Fratta, A. Vagati, and F. Villata. On the evolutino of ac machines for spindle drive applications. *IEEE Transactions on Industry Applications*, 28(5):1081–1086, September/October 1992.

[10] B. Crossland and A.S. Bahrani. *Source Book on Innovative Welding Processes*, chapter Fundamentals of Explosive Welding, pages 99–115. American Society for Metals, 1981.

[11] S.K. Banerjee and B. Crossland. *Source Book on Innovative Welding Processes*, chapter Mechanical Properties of Explosively-Cladded Plates, pages 145–150. American Society for Metals, 1981.

[12] A.H. Burr and J.B. Cheatham. *Mechanical Analysis and Design.* Prentice Hall, 2nd edition, 1995.

[13] A.E. Fitzgerald, Jr. C. Kingsley, and S. D. Umans. *Electric Machinery.* McGraw Hill, 1990.